Evidence for substructure in lens galaxies?

Shude Mao & Peter Schneider
Max-Planck-Institut für Astrophysik
Postfach 1523
D-85740 Garching, Germany

Abstract

We discuss whether one should expect that multiply imaged QSOs can be understood with 'simple' lens models which contain a handful of parameters. Whereas for many lens systems such simple mass models yield a remarkably good description of the observed properties, there are some systems which are notoriously difficult to understand quantitatively. We argue that at least in one case (B 1422+231) these difficulties are not due to a 'wrong' parametrization of the lens model, but that the discrepancy between observed and model-predicted flux ratios are due to substructure in the lens. Similar to microlensing in the optical, such substructure can distort also the radio fluxes predicted by 'simple' mass models, in particular for highly magnified images, without appreciably changing image positions.

1 Introduction

Multiply imaged QSOs and radio (Einstein) rings provide the most accurate mass measures of distant galaxies (Zwicky 1937; for an example, see e.g. Rix, Schneider & Bahcall 1992) and promises to become one of the most robust methods for measuring H_0 (Refsdal 1964; for recent examples, see Falco et al. 1996; Courbin et al. 1997). These successes and expectations are based on our ability to understand the lensing geometry in sufficient detail. It is truly remarkable that many multiple QSOs can in fact be modelled quite accurately with a simple elliptical deflection potential or an elliptical mass distribution. This has nourished the expectation that most lens systems are in fact due to a fairly simple mass distribution (a well-known exception is the system MG2016+112; see Nair & Garrett 1997).

When modelling a multiple QSO lens system, one can either include or exclude the flux ratios of the images. Given that the number of observational constraints in these systems is never much larger than the number of free parameters of the lens model (and often is the same), there is of course a strong motivation to make use of the flux ratio information. As pointed out by Chang & Refsdal (1979), this may be a dangerous undertaking, given that the size of the optical continuum emitting region of QSOs are expected to be of the same order as the Einstein radius of a star in the lens galaxy, so that the optical magnitudes may well be affected by gravitational microlensing (see Wambsganss 1990, and references therein), even if averaged over long periods of time. For example in the case of QSO2237+0305, the image positions can be fitted very accurately with a variety of lens models (e.g., Kent & Falco 1988, Rix et al. 1992, Wambsganss & Paczynski 1994), but the observed optical flux of image D is smaller than predicted, whereas the radio flux ratios (Falco et al. 1996) are in much better accord with the lens models. Therefore, constraints derived from optical fluxes should be used with care only, whereas radio sources are expected to be extended much beyond the Einstein radius of a stellar mass object, so that their flux should be (largely) unaffected by microlensing and thus provide useful constraints for lens modelling.

That argument would of course be weakened if lens galaxies contain mass clumps with an Einstein radius comparable to the size of the radio components – i.e., masses of the order of, or exceeding, globular clusters. In that case the same situation as microlensing in the optical would apply. But this 'milli-lensing' could cause observable image splittings which have not yet been detected, so that this possibility appears not very plausible.

Nevertheless, as we shall argue in Sect. 2, the difficulty to model some lens systems in detail, with radio flux ratios included, points towards substructure in lens galaxies (or somewhere else along the line-of-sight to the QSO). Two kinds of substructure are briefly considered in Sect. 3, and numerical experiments to determine the probability for appreciable flux-ratio changes are presented in Sect. 4. We summarize our conclusions in Sect. 5, together with a suggestion how to treat (radio) flux ratios in lens modelling.

2 B1422+231: More than a challenge for lens modellers

The quadruply imaged QSO 1422+231 was discovered in the course of the JVAS survey (Patnaik et al. 1992). The four images have a maximum separation of $1\farcs3$, and the lens galaxy has been accurately located recently (Impey et al. 1996). The flux ratios of the images are different in the radio and optical band; in the radio, they are A:B:C:D= 0.98:1:0.52:0.02, whereas in the optical, image A is fainter relative to B, yielding A:B$\approx$0.8, somewhat dependent on the optical filter (the radio flux ratios are nearly independent of radio frequency), whereas the B:C:D ratio is compatible with that in the radio. Given that the optical flux may be affected by microlensing and/or dust obscuration, the radio flux ratios should be used in modelling this system.

Several serious attempts have been made to model the lens in this system (e.g., Hogg & Blandford 1993, Kormann, Schneider & Bartelmann 1994b, Keeton, Kochanek & Seljak 1996) – and they all failed! Whereas the image positions can be fitted very accurately, the radio flux ratio could not be obtained. Given that the parametrized lens models used by the different authors were quite different, this failure is probably not due to a 'stupid' choice of family of lens models, but is a generic difficulty for 'simple' (i.e., smooth) lens models, as can be seen as follows:

The large flux ratio between the images A, B, C, and the image D of ~ 50 leaves the two possibilities that (i) image D is highly demagnified, or (ii) that A, B, C are highly magnified. We can exclude option (i), since the separation of D from the center of the lens galaxy – $0\farcs3$ – does not put it into a region of very high surface mass density necessary to obtain a strong demagnification. This thus leaves only option (ii). The generic situation in which three highly magnified images occur is when a source is close to, and inside a cusp (see Chap. 6 of Schneider, Ehlers & Falco 1992). In that case, there exists a universal relation between the image fluxes (see, e.g., Schneider & Weiss 1992; Mao 1992), namely that the sum of the fluxes of the outer two images (A and C) should equal the flux of the middle image (B). This relation is grossly violated in 1422+231, although the VLBI structure shows strong elongation in the direction tangent to the direction of the lens galaxy which supports the cusp hypothesis. Hence, although this universal relation is strictly valid only asymptotically for very high magnification, or in other words, if the source is sufficiently close to the cusp (and the theory of the lens mapping near cusps developed so far does not provide a good handle of where the 'asymptotic regime begins'), this argument easily explains why all the published lens models yield flux ratios with (A+C)/B$\lesssim$1.3 (the observed value in radio is 1.5). A strong violation of the cusp constraint can be obtained by either putting the source further away from the cusp – but that would decrease the magnification, thus the magnification ratio to D, therefore running into the same problem as for option (i) above – or to impose a small-scale structure on the lens model which can locally change the magnification of individual images. Here, small scale means a scale smaller than the separation between A, B, and C, i.e., smaller than $\sim 0\farcs5$.

Although B1422+231 is the system where the problems of modelling are most easily seen, it is probably not unique. Keeton et al. (1996) and Falco, Lehár & Shapiro (1996) have modelled MG0414+0534, and in both attempts the resulting χ^2 per degree of freedom is too large to view these models as satisfying. In this system, the components A1 and A2 have a separation much smaller than to the other two components, which suggests that they are close to a critical curve passing between them. In that case, one would expect that the fluxes of A1 and A2 were much larger than those of B and C, and that the flux ratio A1/A2 would be of order unity. This expectation is not at all satisfied with the optical data, and one should therefore not be surprised to find the 'simple' models fail (for this case, microlensing by stellar mass objects offers a plausible explanation, Witt, Mao & Schecter 1995). A similar situation occurs in PG1115+080 (Keeton & Kochanek 1996) where all χ^2 of their best fits comes from the flux ratio of A1/A2, which is significantly different from unity (Courbin et al. 1997). We consider these difficulties as a hint towards substructure in the lens galaxy. In the next two section, we shall show how small amplitude 'perturbations' of the mass distribution in the lens is sufficient to lead to the observed discrepancies.

3 Analytic estimates

We shall consider two particular hypotheses for the kind of substructure that may be present in a lens galaxy like that in B1422: globular clusters (or in lensing language: point masses of order $10^6 M_\odot$), and small amplitude fluctuations.

3.1 The 'globular cluster' picture

A point mass of $\sim 10^6 M_\odot$ yields a deflection angle at its Einstein radius of about 1 milli-arcsecond, and thus can cause multiple images with similar separation, provided that source and lens are sufficiently well aligned. Since we are interested in some small perturbation of the magnification of a macroimage, the typical situation will be one where the separation of the point mass from the image is considerably larger than the Einstein radius, so that the deflection angle is also smaller, and the secondary image will be highly demagnified.

Consider a macroimage with local surface mass density κ_0 and shear γ_0, with coordinates chosen such that only the 1-component of the shear caused by the macro-model is non-zero. Let a point mass be located at position $(x\cos\varphi, x\sin\varphi)$ relative to the image, where x is measured in units of the Einstein radius of the point mass. The unperturbed and perturbed magnifications are then, respectively,

$$\mu_0 = \frac{1}{(1-\kappa_0)^2 - \gamma_0^2} \quad ; \quad \mu = \frac{1}{(1-\kappa_0)^2 - (\gamma_0 + \delta\gamma_1)^2 - \delta\gamma_2^2} \ , \tag{1}$$

where $(\delta\gamma_1, \delta\gamma_2) = (\cos 2\varphi, \sin 2\varphi)/x^2$ is the shear caused by the point mass lens. Let $R = \mu_0/\mu$ be the ratio of the unperturbed to the perturbed magnification; its dependence on x and φ can be written as

$$x^2 = \frac{\gamma_0 \mu_0 \cos 2\varphi}{1-R} \left(1 + \sqrt{1 + \frac{1-R}{\mu_0 (\gamma_0 \cos 2\varphi)^2}} \right) \approx \frac{2\gamma_0 \mu_0 \cos 2\varphi}{1-R} \ , \tag{2}$$

where in the second step we assumed that $|1-R| \ll 1$, since we are interested in small magnification perturbations. Thus, locations $\mathbf{x}$ of the point mass for constant flux perturbation R trace an '∞'-like curve. The area of the region in which a point mass has to be located in order to cause a flux perturbation larger (smaller) than R for $R > 1$ ($R < 1$) is

$$A = 2 \left| \gamma_0 \frac{\mu_0}{1-R} \right| \ , \tag{3}$$

as can be easily obtained from integrating (2) over φ. For the lens models applicable to 1422, the A image should have $\mu_0 \sim 15$, $\gamma_0 \sim 0.5$, and so the area in which a point mass lens has to be located to cause a flux perturbation of $\pm 20\%$ is $A \sim 150$. Thus, with a surface mass density $\kappa_* \sim 0.02$, one obtains a high probability to find one of these point-mass lenses inside the region where it causes an appreciable magnification change.

3.2 Plane wave perturbations

As a second 'model' for lens perturbations, we consider a plane density wave. For simplicity of the argument, we again assume that the shear caused by the macromodel has only a 1-component, and that the plane wave is modulated also in the 1-direction. Then, $\delta\kappa = \delta\gamma_1$, $\delta\gamma_2 = 0$. The ratio R then becomes, up to first order in the perturbation $\delta\kappa$,

$$R = 1 - \delta\kappa \frac{2}{1 - \kappa_0 - \gamma_0} \ . \tag{4}$$

The denominator in (4) is one of the eigenvalues of the magnification matrix caused by the macromodel. For images near a critical curve, one of the eigenvalues becomes very small, so that R can deviate significantly from unity even for small $\delta\kappa$. For the A image of 1422, one expects $\kappa_0 + \gamma_0 \approx 0.9$, so that for a 20% change in magnification one needs $\delta\kappa \sim 0.01$, a truly small fluctuation.

4. Numerical Simulations

We model the primary lensing galaxy G1 as a singular isothermal ellipsoid (SIE) density distribution and take into account the effect of several nearby galaxies as an external shear (Kormann, Schneider & Bartelmann 1994b). The external shear may also include contributions from large scale structure and/or the deviation of the primary lens galaxy from the SIE model. We choose the coordinate system on the lens plane, $\mathbf{x} = (x_1, x_2)$, centered on the primary lens galaxy, with the x_1-axis along (decreasing) right ascension and the x_2-axis along (increasing) declination. The corresponding positions in the source plane $\mathbf{y} = (y_1, y_2)$ have the same orientations. All the length units are expressed in arcseconds, and the surface density in units of the critical surface density, $\Sigma_{\rm cr}$. For an Einstein-De Sitter universe, $1'' = 3.8h^{-1}$kpc at the lens plane, and the critical surface density is $\Sigma_{\rm cr} = 3500hM_\odot/{\rm pc}^2$, here h is the present-day Hubble constant in units of 100 km s^{-1} Mpc^{-1}.

If the minor axis of the lens is along the x_1-axis, the SIE potential can be written as

$$\psi_g(x,\phi) = \theta_0 x \frac{\sqrt{f}}{f'} \times [\sin\phi \ \arcsin(f'\sin\phi) + \cos\phi \ {\rm arcsinh}\ (\frac{f'}{f}\cos\phi)] \ , \tag{5}$$

where f is the axis ratio, $f' = \sqrt{1-f^2}$, θ_0 is an angle that specifies the strength of the lens potential, and we have used polar coordinates $\mathbf{x} = (x\cos\phi, x\sin\phi)$. The shear perturbation is given by

$$\psi_\gamma(x,\phi) = \frac{x^2}{2}\gamma\cos(2\phi) \ , \tag{6}$$

if the shear direction is along the x_1-axis. The total potential is the sum of the SIE potential and the shear perturbation,

$$\psi_0 = \psi_g(x, \phi-\phi_g) + \psi_\gamma(x, \phi-\phi_s) \ , \tag{7}$$

where we have now generalized to the case when the lens minor axis encloses an angle ϕ_g, and the direction of shear an angle of ϕ_s with the x_1-axis. The lens equation is then simply: $\mathbf{y} = \mathbf{x} - \nabla\psi(\mathbf{x})$. The Jacobian of the lens mapping is $\mathcal{A} = \partial\mathbf{y}/\partial\mathbf{x}$, and the magnification of an image is given by $\mu = ({\rm det}\mathcal{A})^{-1}$. We refer the readers to Kormann et al. (1994a,b) for more technical details.

4.1 A macromodel

Observational data is taken from Tables 1 and 2 in Impey et al. (1996). The total number of observational constraints is 11, namely we have 4×2 image positions and 3 relative flux ratios. In comparison, our lens model is described by 7 parameters, i.e., three lens parameters, (ϕ_g, f, θ_0), two shear parameters, (γ, ϕ_s), and two source coordinates. Thus, the number of degrees of freedom is 4. Nearly identical procedures as in Kormann et al. (1994b) are used to find the best lens model. A minor difference is that we have only included the flux ratio D:B in the χ^2 measure, since we argued that substructures may have modified flux ratios of the brighter images significantly. There are a few models that can fit the data with acceptable χ^2 (cf. Keeton et al. 1996). One of these is summarized in Table 1. The model reproduces the observed positions within 1σ of the observed uncertainties. The relative magnifications are, however, unsatisfactory. The flux ratio A:B is 0.78, close to the observed optical flux ratio, but deviates significantly from the observed radio value 0.98. In addition, image D is too bright compared with the observed value.

Table 1: Model Parameters

θ_0	f	ϕ_g	γ	ϕ_s	μ_A	μ_B	μ_C	μ_D
0.77	0.78	-1.01	0.20	-1.04	7.01	-9.01	4.52	-0.33

4.2 The 'globular cluster' picture

The presence of massive lenses with mass $\sim 10^6 M_\odot$ provides a perturbation potential:

$$\delta\psi \propto \sum \frac{1}{2} \ln[(x - x_i)^2 + (y - y_i)^2] \tag{8}$$

on top of ψ_0. For simplicity we assume that these lenses are uniformly distributed and have a surface density of κ_* in units of the critical surface density. Similar to microlensing by solar mass objects (Wambsganss 1990), we generate point lenses randomly on the lens plane with the required surface density. To quantify the deviation of magnifications from that of the unperturbed potential, we define a quantity $r = (\mu_A + \mu_B + \mu_C)/(|\mu_A| + |\mu_B| + |\mu_C|)$. If the magnifications of image A, B and C strictly obey the prediction of the cusp singularity, $r = 0$. The input value resulting from the unperturbed potential ψ_0 is $r = 0.123$. In Fig. 1, we show the probability distribution of r from Monte Carlo simulations. For $\kappa_* = 0.005, 0.01$, the probability of having a deviation larger than the observed one is about 21% and 36%. Therefore, a surface density in 'globular clusters' ≈ 0.005 may be sufficient to explain the observed deviation in flux ratios. Nearly in all the cases, the change in the image positions are of a few milli-arcsecond. Such small changes are undetectable in the optical. In any case, such small changes can probably be accommodated by a small adjustment in the macromodel.

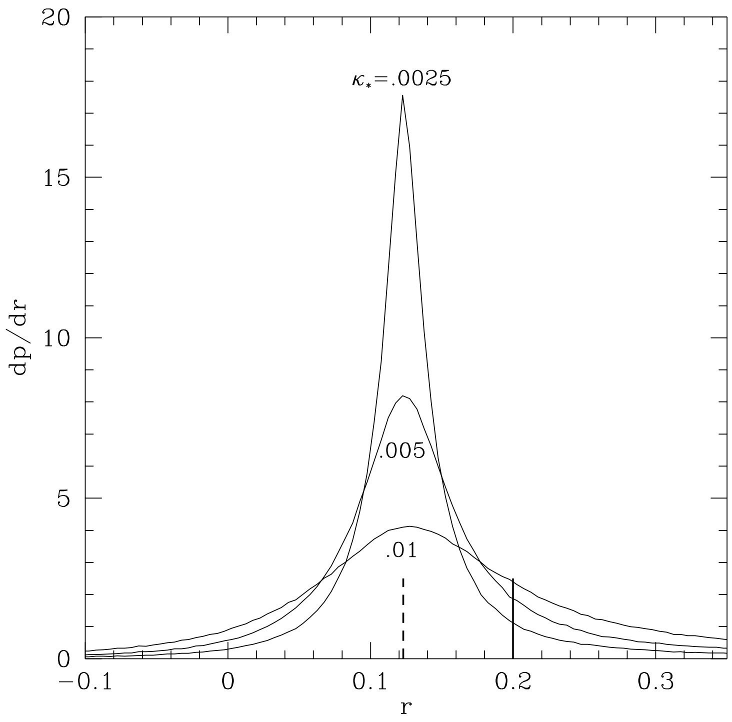

Fig. 1. Probability distribution for the quantity $r = (\mu_A + \mu_B + \mu_C)/(|\mu_A| + |\mu_B| + |\mu_C|)$ for a singular isothermal ellipsoid with external shear and massive point lenses. r measures the deviation of magnifications from the prediction ($r = 0$) of a cusp singularity. Equal-mass point lenses are distributed uniformly with surface density κ_*. The dashed vertical line indicates the input value for the unperturbed lens model. The solid vertical line shows the observed value of $r = 0.2$. Three curves are shown for $\kappa_* = 0.0025, 0.005, 0.01$. The probability of having a deviation larger than the observed one is (11, 21, 36)% for $\kappa_* = 0.0025, 0.005, 0.01$, respectively.

4.3 Plane wave perturbation

For each image, we consider a plane-wave fluctuation centered on the image described by

$$\delta\psi = \frac{A}{k^2}\cos(k_1x_1 + k_2x_2 + \phi_0)e^{-\frac{x^2}{2\sigma_r^2}} \,, \tag{9}$$

where A is the amplitude of fluctuation, (k_1, k_2) is the wave vector, ϕ_0 is a phase constant, and the last term localises the perturbation within a few σ_r. Notice that in the absence of the last term, the amplitude of the surface density corresponds to $\delta\psi$ is $A/2$. Since the parameter space is rather large, we limit our study to one illustrative case. We fix the magnitude of the wave-vector to be $2\pi/|k| = 0\overset{''}{.}01$ but with random orientations. ϕ_0 is distributed uniformly between 0 to 2π, and the amplitude of fluctuations is drawn from a Gaussian distribution with standard deviation σ. We take $\sigma_r = 0\overset{''}{.}01$, but the results are insensitive to the choice of σ_r. In Fig. 2, we show the probability distribution of r for $\sigma = 0.01, 0.02, 0.03$. The probability of having deviations larger than the observed one is (0.6, 4.6, 8.3)% for $\sigma = 0.01, 0.02$, and 0.03 respectively. These values are in good agreement with the analytical estimates presented in section 3.

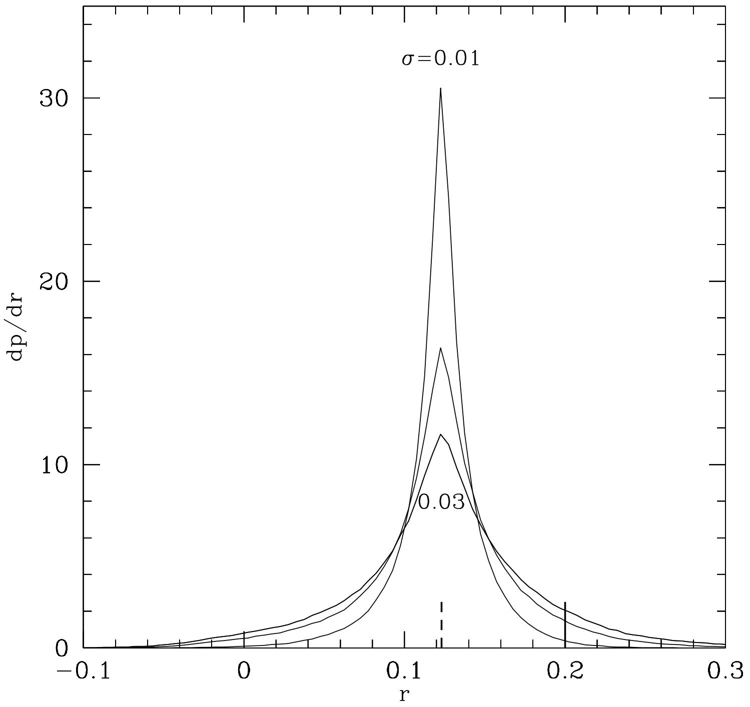

Fig. 2. Probability distribution for the quantity $r = (\mu_A + \mu_B + \mu_C)/(|\mu_A| + |\mu_B| + |\mu_C|)$ for a singular isothermal ellipsoid with external shear and localised plane-wave fluctuations. The amplitude of fluctuations is drawn from a Gaussian distribution with standard deviation σ. Three curves are shown with $\sigma = 0.01, 0.02, 0.03$. The probability of having deviations larger than the observed one is (0.6, 4.6, 8.3)% for $\sigma = 0.01, 0.02$, and 0.03, respectively. The dashed and solid lines have the same meaning as in Fig. 1.

5 Summary and Discussion

We have discussed the possibility that the flux ratios in lens systems may be affected by small scale structure in the lens galaxy. A general analytic argument was presented why 'simple' lens models are unable to account for the radio flux ratios in B1422+231, and we considered two potential pictures for substructure, namely 'globular clusters' with $\sim 10^6 M_\odot$ and smooth perturbations, modelled as plane density waves. We have considered both pictures analytically, as well as through numerical simulations. Owing to the large magnifications of images A, B, C in 1422, only small perturbations (in mass) are needed to change magnifications, and thus flux ratios appreciably. The required perturbation is of the order of $\sim 1\%$ of the critical surface density, or about $(35hM_\odot \mathrm{pc}^{-2})$ in physical units. There are about 200 globular clusters in the Galaxy with a total mass of $\approx 10^8 M_\odot$. These globular clusters form a quasi-spherical distribution concentrated toward the galactic center. The average surface density of these objects within 5kpc is $\sim 1M_\odot \mathrm{pc}^{-2}$, this is $3\times10^{-4}h^{-1}$ of the critical surface density, somewhat too low to produce significant change in magnification (cf. Fig. 1). The 'globular cluster' picture should apply equally well to the hypothetical massive black holes in galactic halos (e.g., Lacey & Ostriker 1985). They can produce much more visible deviations if they contribute just a few percent of mass in halos. Our second model of substructure addresses smooth fluctuations. Such smooth inhomogeneity is quite naturally expected in hierarchical structure formation models as a result of continuous merging and accretion processes.

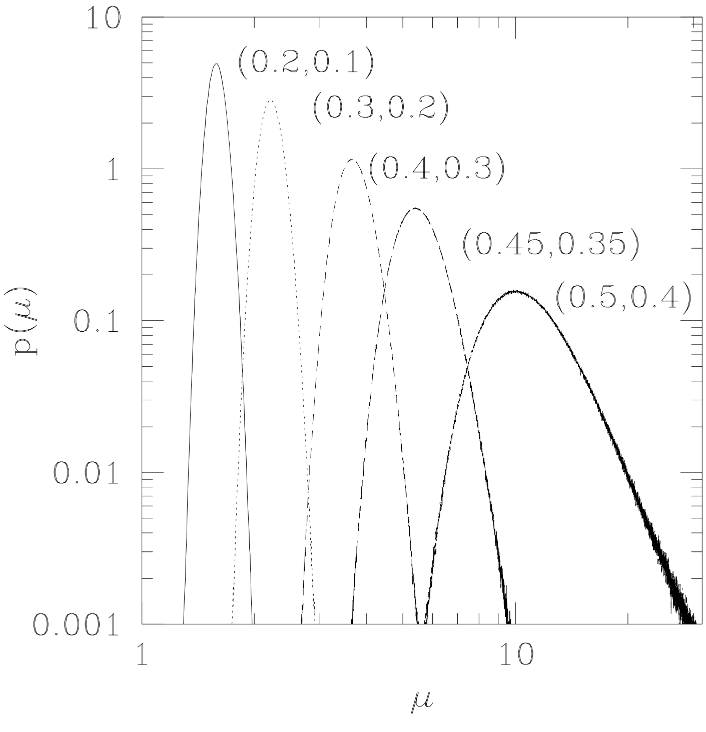

Fig. 3. The probability density $p_\mu(\mu)$, for five pairs of (κ_0, γ_0) of the macromodel, as indicated near the curves. The probability density for the perturbations $\delta\kappa$ and $\delta\gamma$ have been assumed to follow a Gaussian, with width $\sigma_\kappa = \sigma_\gamma = 0.02$. It is easily seen that images with higher magnifications attain a much broader magnification distribution than those where the magnification is of order unity.

Although we have discussed only the SIE model, we have verified that it is still difficult to fit the observed flux ratios using other parametrizations of the deflection potential. If we accept the view that the surface mass density of lens galaxies is not as smooth as described by 'simple' lens models, using flux ratios for modelling may yield misleading conclusions. On the other hand, discarding them totally would be foolish, since as long as the perturbations are small, the magnification is only weakly affected for images which are not highly magnified. Therefore, a statistical treatment may be appropriate: Let $p_\mu(\mu;\kappa,\gamma)$ be the probability density for a magnification μ, given that the smooth model has surface mass density κ and shear γ. For example, assuming that the perturbations $\delta\kappa$ and $\delta\gamma$ are drawn from a Gaussian distribution of width σ_κ and σ_γ, one can easily calculate p_μ; an example is provided in Fig. 3. Then, for N images with observed positions $\boldsymbol{\theta}_I^{(\mathrm{obs})}$, positional uncertainty σ_i, and observed fluxes S_i, the likelihood function that can be maximized for obtaining good fits is

$$\mathcal{L} = \prod_{i=1}^{N} \frac{1}{\pi\sigma_i^2} \exp\left(-\frac{\left|\boldsymbol{\theta}_i - \boldsymbol{\theta}_i^{(\mathrm{obs})}\right|}{\sigma_i^2}\right) p_\mu\left(\frac{S_i^{(\mathrm{obs})}}{S_0};\kappa_i,\gamma_i\right) , \tag{10}$$

where $\boldsymbol{\theta}_i$, κ_i, and γ_i are the predicted image positions, surface mass density and shear at these positions, and S_0 is the unlensed source flux. If the uncertainty in the flux measurements are larger than the width of p_μ, then the function p_μ should be convolved with a Gaussian of width δS_i. Given the generally expected shape of p_μ, the fluxes of weakly magnified images provide strong constraints, whereas highly magnified images yield weaker constraints on the model.

We thank Hongsheng Zhao for helpful discussions. This work was supported by the "Sonderforschungsbereich 375-95 für Astro–Teilchenphysik" der Deutschen Forschungsgemeinschaft.

References

Chang, K. & Refsdal, S. 1979, Nature, 282, 561

Courbin, F., et al. 1997, astro-ph/9705093.

Falco, E.E., Lehár, J. & Shapiro, I.I. 1996, astro-ph/9612182.

Falco, E.E., Shapiro, I.I., Moustakas, L.A. & Davis, M. 1997, astro-ph/9702152

Hogg, D.W. & Blandford, R.D. 1994, MNRAS, 268, 889

Impey, C.D., Foltz, C.B., Petry, C.E., Browne, I.W.A. & Patnaik, A.R. 1996, ApJ, 462, L53

Keeton II, C.R., Kochanek, C.S. 1996, astro-ph/9611216

Keeton II, C.R., Kochanek, C.S. & Seljak, U. 1996, astro-ph/9610163

Kent, S.M. & Falco, E.E. 1988, AJ, 96, 1570

Kochanek, C.S. 1991, ApJ, 373, 354

Kormann, R., Schneider, P. & Bartelmann, M. 1994a, A&A, 284, 285

Kormann, R., Schneider, P. & Bartelmann, M. 1994b, A&A, 286, 357

Lacey, C. G. & Ostriker, J. P. 1985, 290, 154

Mao, S. 1992, ApJ, 389, 63

Nair, S. & Garrett, M.A. 1997, MNRAS 284, 58.

Patnaik, A.R. et al. 1992, MNRAS, 259, 1P (P92)

Refsdal, S. 1964, MNRAS, 128, 307

Rix, H.-W., Schneider, D.P. & Bahcall, J.N. 1992, AJ, 104, 959

Schneider, P., Ehlers, J. & Falco, E. E. 1992, *Gravitational Lenses* (Springer-Verlag: New York)

Schneider, P. & Weiss, A. 1992, A&A, 260, 1

Wambsganss, J. 1990, report MPA 550, Garching

Wambsganss, J. & Paczyński, B. 1994, AJ, 108, 1156

Witt, H.J., Mao, S. & Schechter, P. 1995, ApJ, 443, 18

Zwicky, F. 1937, Phys. Rev., 51, 290